

This work was written as part of one of the author's official duties as an Employee of the United States Government and is therefore a work of the United States Government. In accordance with 17 U.S.C. 105, no copyright protection is available for such works under U.S. Law.

Public Domain Mark 1.0

<https://creativecommons.org/publicdomain/mark/1.0/>

Access to this work was provided by the University of Maryland, Baltimore County (UMBC) ScholarWorks@UMBC digital repository on the Maryland Shared Open Access (MD-SOAR) platform.

Please provide feedback

Please support the ScholarWorks@UMBC repository by emailing scholarworks-group@umbc.edu and telling us what having access to this work means to you and why it's important to you. Thank you.

Detection of initial damage in Norway spruce canopies using hyperspectral airborne data

P. K. ENTCHEVA CAMPBELL*, B. N. ROCK, M. E. MARTIN

Complex Systems Research Centre, University of New Hampshire, Durham,
NH 03824, USA

C. D. NEEFUS

Department of Plant Biology, University of New Hampshire, Durham,
NH 03824, USA

J. R. IRONS, E. M. MIDDLETON

Biospheric Sciences Branch, NASA Goddard Space Flight Center, Greenbelt,
MD 20771, USA

and J. ALBRECHTOVA

Department of Plant Physiology, Charles University, 12844 Prague 2,
Czech Republic

(Received 5 February 2003; in final form 19 April 2004)

Abstract. Current broadband sensors are not capable of separating the *initial* stages of forest damage. The current investigation evaluates the potential of hyperspectral data for detecting the initial stages of forest damage at the canopy level in the Norway spruce (*Picea abies* (L.) Karst) forests of Czech Republic. Hyperspectral canopy reflectance imagery and foliar samples were acquired contemporaneously for 23 study sites in August 1998. The sites were selected along an air pollution gradient to represent the full range of damage conditions in even-aged spruce forests. The changes in canopy and foliar reflectance, chemistry and pigments associated with forest damage were established. The potential of a large number of spectral indices to identify initial forest damage was determined. Canopy hyperspectral data were able to separate healthy from initially damaged canopies, and therefore provided an improved capability for assessment of forest physiology as compared to broadband systems. The 673–724 nm region exhibited maximum sensitivity to initial damage. The nine spectral indices having the highest potential as indicators of the initial damage included: three simple band ratios, two derivative indices, two modelled red-edge parameters and two normalized bands. The sensitivity of these indices to damage was explained primarily by their relationship to foliar structural chemical compounds, which differed significantly by damage class.

*Author for correspondence at: NASA Goddard Space Flight Center Code 923, Greenbelt, MD 20771, USA; e-mail: pcampbel@pop900.gsfc.nasa.gov

1. Introduction

Maintaining healthy and functional forests is important because forests are one of the major terrestrial CO₂ sinks and local atmospheric O₂ sources. A decline in forest health can result in abnormal reductions in forest ecosystem productivity and diversity and could cause a significant effect on the terrestrial biogeochemical cycling. Because forests cover approximately 40% of the Earth's ice-free land surface (Waring and Running 1998), remote sensing-based forest monitoring is of critical importance for assessing forest health worldwide. Effective forest monitoring and timely forest management decisions for remediation require the early detection of forest damage due to either natural or anthropogenic factors.

High elevation spruce forest ecosystems are highly sensitive to environmental and climatic changes (National Acidic Precipitation Assessment Program (NAPAP) 1990). The Norway spruce forests (*Picea abies*) of Central Europe have exhibited a dramatic growth decline due to high levels of air pollution (including SO₂, NO_x, and O₃), beginning in approximately 1965 (Kubikova 1991). The high elevation forests located in the Krushne hory mountains, northern Bohemia along the borders of the Czech Republic and Germany, grow in one of the most heavily polluted regions of the world (Materna 1989, Kubikova 1991, Klasterska 1991, Klimont *et al.* 1993, Ardo *et al.* 1997). Air pollution has altered the ecosystem conditions in this region directly and by causing soil acidification (Kubikova 1991, Ardo *et al.* 1997). The Krusne hory mountains offer a unique opportunity to study the full range of forest damage conditions within a simple, homogeneous Norway spruce ecosystem, located within a narrow elevational range and along a sharp air pollution gradient.

Canopy level vegetation spectral properties are determined by a combination of factors, including canopy density and structure, foliar pigment levels, water content and biochemical constituents (Rock *et al.* 1986, 1988, Martin and Aber 1997). Differences in the canopy structure, amount of foliage and foliar constituents within a single species are indicative of differences in forest health. Foliar chlorophyll and carotenoid concentrations typically decrease in response to stress while additional foliar compounds may accumulate within the leaves. Such changes affect foliar spectral properties, providing potential for remote sensing diagnosis of vegetation stress (Rock *et al.* 1986, Martin 1994, Martin and Aber 1997). Foliar structural chemistry (cellulose and lignin) is indicative of the growing conditions at the time of needle formation, since cell wall composition does not change over time, as growing conditions degrade or improve (McNulty *et al.* 1991). Foliar photosynthetic pigment concentrations (chlorophyll *a* and *b*, carotenoids) are dynamically responsive to current climate and soil conditions. Thus, remote sensing (RS) monitoring of canopy vigour based on estimates of structural chemical constituents may allow for forest health monitoring and damage detection of the long-term environmental conditions, while the differences in foliar pigment levels would be indicative of the near-term growing environment (shortly before the data acquisition).

Forest damage classifications separate forest stands into five or six physiologically based categories (Hildebrandt and Gross 1992). However, the commonly available multispectral sensors (>20 nm bandwidth) can discriminate only very broad categories of forest damage (healthy, dead and intermediate), which are too general to be applicable in forestry practices (Rock *et al.* 1993, Lambert *et al.* 1995, Ardo *et al.* 1997). Lambert *et al.* (1995), for example, used Landsat Thematic Mapper (Landsat TM) to discriminate three levels of forest damage: healthy/light

damage, moderate damage and heavy damage/dying. Due to the broad spectral bands and the 30-m pixel size, identification of the initial levels of damage in Norway spruce was not achieved. However, high spectral and spatial resolution data might provide the means for RS separation of physiologically defined forest damage classes. High spectral resolution data have been used to characterize both foliar and canopy pigment levels (Rock *et al.* 1988, Chappelle *et al.* 1992, Miller *et al.* 1993) and biochemistry (Bolster *et al.* 1996, Martin and Aber 1997, Martin 1994). Hyperspectral systems that acquire data in the visible and the near infrared may allow for the monitoring of early stages of damage in vegetation characterized by reductions in chlorophyll concentrations (Rock *et al.* 1988, Miller *et al.* 1993).

Many of the analyses and algorithms developed using high spectral resolution data are based on leaf-level reflectance measurements and assessments of foliar pigments. Such algorithms need to be applied to spectra acquired at the forest stand level; and their potential for damage detection at the canopy level should be assessed (Datt 1998). The sensitivity of such algorithms to changes in pigment concentration and foliar chemical constituents occurring along a vegetation damage gradient have not been evaluated previously.

The goal of this investigation was to evaluate the potential of airborne hyperspectral remote sensing data for identifying the initial levels of damage in Norway spruce canopies along an air pollution gradient. The objectives of the research were:

- 1) to evaluate the canopy-level spectral reflectance properties of Norway spruce across a full range of damage levels and determine the visible and near infrared spectral regions most sensitive to damage discrimination;
- 2) to evaluate the potential of the reflectance indices derived from the airborne dataset for separation of the initial damage levels from healthy and moderately damaged classes; and
- 3) to determine the relationships among spectral reflectance indices and forest canopy biophysical parameters.

2. Methodology

2.1. Study area

The high elevation forests of the Krusne hory, located along the Czech–German border (figure 1), offer for the current study a unique opportunity to study the full gradient of forest decline conditions across a homogeneous Norway spruce ecosystem, within a limited elevation range (900–1000 m) and across a spatial transect of approximately 50 km from west (healthy and initial damage) to east (severe damage). This area was used in previous Landsat TM forest damage assessments (Lambert *et al.* 1995, Ardo *et al.* 1997). Those earlier investigations identified elevation as a significant factor associated with forest decline, with lower-elevation sites (≤ 800 m) less damaged than upper-elevation sites (≥ 1000 m) (Rock *et al.* 1986, 1988, 1992, 1993, Moss and Rock 1991, Moss *et al.* 1998). The study areas (figure 1) have undergone detailed soil and forest surveys and climate monitoring by the Czech Forest Service (Henzlik 1997). With this investigation, air quality was not evaluated. Air pollution due to fossil fuel burning (predominantly SO₂, NO_x, and O₃) has been thoroughly documented and monitored in the area (Materna 1989, Klasterska 1991, Kubikova 1991, Klimont *et al.* 1993, Henzlik 1997), and therefore is assumed to be the major forest stress agent.

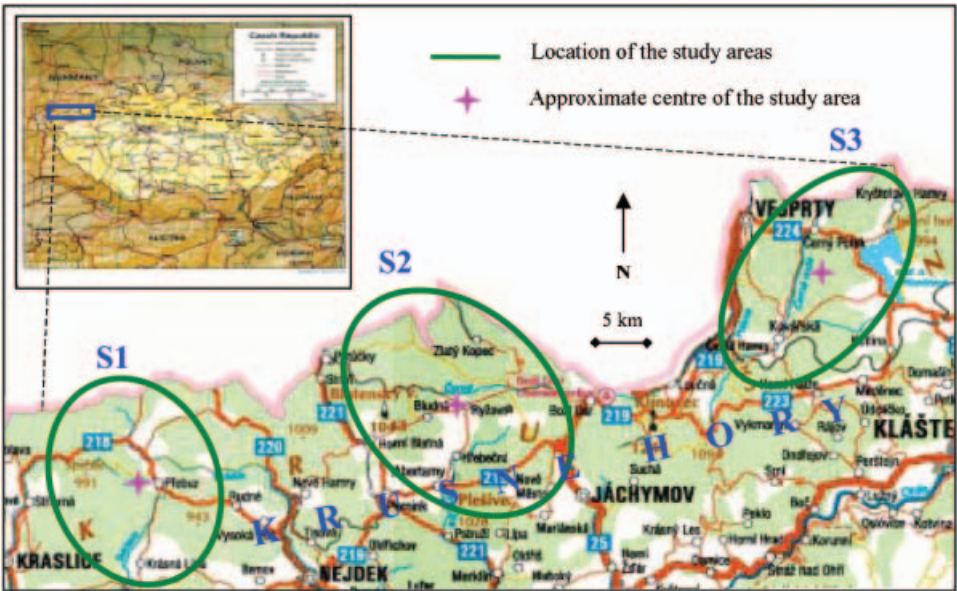


Figure 1. Location of the study areas in the Krusne hory, Czech Republic: Norway spruce forests representing the full range of forest health conditions (DC0–DC3) due to SO₂ pollution. The locations of the study areas and ASAS flight lines are indicated as S1 (mostly DC0 and DC1), S2 (mostly DC2, some DC1 and DC3) and S3 (mostly DC3, some DC2). The approximate geographic locations of the centres of the study areas are as follows (latitude and longitude (DD MM SS, WGS84)): S1—50 25 32, 12 37 27; S2—50 31 15, 12 52 15; S3—50 47 30, 13 06 30.

2.2. Evaluation of forest damage level

Forest physiological condition was assessed using a methodology for evaluating the state of individual tree crowns established by Hildebrandt and Gross (1992) for use with colour infrared photography and forest field survey. The procedure was modified for use with high spectral resolution digital imagery and forest field surveys (Entcheva *et al.* 1996). The modified field procedure initially assigned individual tree crowns into one of five damage categories (table 1) ranging from healthy to dead. Next, the crown characteristics of a stand were summarized to classify whole stands into damage levels. The primary factors for field determination of damage class included: (1) crown thinning characteristics—crown type (i.e. brush, comb or plate; Hildebrandt and Gross 1992), form and

Table 1. Forest damage evaluation criteria and damage level assignment.

Damage class (DC)	Ecosystem vitality status	Canopy defoliation ^a (%)	
		Chlorosis absent	Chlorosis present
0	Healthy	0–10	—
1	Initial damage	11–25	0–10
2	Medium damage	26–60	11–25
3	Heavy damage	61–80	26–60
4	Ecosystem collapse ^b	81–100	61–100

^aCharacteristics of more than 70% of the trees within the stand.

^bAt this stage more than 50% of the trees within the stand are dead.

shape; (2) percentage foliar loss; (3) presence/absence of chlorosis; and (4) foliar retention. The current research focused on the discrimination of the initial stages of forest damage (DC1) from healthy (DC0) and moderate damage (DC2 and DC3), so dead stands were excluded from the study, resulting in a classification scheme with four categories (table 1).

2.3. Site selection and forest stand measurements

Even-aged forest stands older than 60 years and larger than five hectares were selected to test the discrimination capabilities of hyperspectral data for initial forest damage detection over the full range of forest health (healthy, initial damage, intermediate and heavy damage). All stands were located along a limited elevation range (within approximately 100 m). Within the three research areas (S1, S2, and S3), 51 30 m × 30 m study sites were randomly selected (figure 1). Five trees within each of the sites, representative of the stand damage level and growth parameters, were selected and marked permanently with aluminium tags. These trees were used for foliar sample collections (table 2).

At the centre of each site, differentially corrected GPS coordinates were recorded, and stand structure and damage class were determined. Within an 11.3-m radius circular plot located at the centre of the study site, forest stand parameters (e.g. stand density, basal area (BA), tree diameter at breast height (DBH), tree height, etc.) were measured (table 2).

2.4. Collection of foliar samples

Foliar sampling was completed within the period 15–28 August 1998. Branch samples from the upper canopy were collected from each of the five representative trees. Two separate sets of foliar samples were collected from the same branch: (1) a set for fresh foliage spectral measurements and determination of foliar lignin, cellulose and nitrogen levels, and (2) a second fresh set for foliar photosynthetic pigment analysis (table 2).

2.5. Foliar spectral measurements and laboratory analysis

The set of samples for fresh foliage spectral measurements and canopy chemistry were immediately sealed in zip-lock plastic bags with wet paper towels, placed in coolers on frozen blue ice and taken to the field laboratory for spectral scanning (within 1–2 hours of collection). The relationship foliar spectra to bio-physiology parameters and forest damage are examined separately (Entcheva 2000).

2.5.1. Dry foliage: NIR analysis for determination of foliar chemical content (relative %)

The samples used for foliar spectral measurements were air-dried, and then the foliage was separated from the branch segments. The spruce needles were ground into 1 mm particle size and used for determination of foliar chemical content. Foliar constituent analyses were performed on a subset of 50 samples, using a series of extractions following the methods described by Newman *et al.* (1994). Standard NIR procedures were used on the complete set of samples to determine the following four categories of chemical compounds: (1) relative amounts of non-polar organic components (fats, waxes and other soluble materials); (2) polar organic extractives (phenols, simple sugars, starch and simple amino acids); (3) cellulose

Table 2. Data collected at the study areas in north-west Bohemia, Czech Republic, August 1998.

Data	Acquisition approach	Study sites/samples
<i>1. Stand and site level measurements and data collections</i>		
ASAS ^a imagery	ASAS, nadir imagery, 60~10 nm bands	23 sites (10 DC0, 5 DC1, 4 DC2, 4 DC3)
GER2600 ^{bc} calibration spectra	Spectra from dark and bright ground targets	Six targets
Field sites sampled	30 m × 30 m sites into 90 m × 90 m homogenous forest areas	51: 14 DC0, 12 DC1, 14 DC2, 12 DC3
Determination of forest damage class	Table 1 (DC0, DC1, DC2 and DC3)	51 sites
Forest canopy closure	Within 1/10 acre plot, forest densiometer	51 sites
Stand density	Within 1/10 acre plot, prism	51 sites
Site GPS position	Field visit, Trimble GPS units	51 sites
Site elevation and map location	Survey maps, Trimble GPS units	51 sites
<i>2. Individual tree and sample level measurements and data collections</i>		
Individual trees damage class	Table 1 (DC0, DC1, DC2 and DC3)	51 sites, five trees per site
Tree diameter at breast height	Tree diameter at 1.30 m height, DBH tape	255 trees
Tree height	Height of the five representative trees, clinometer	255 trees
Tree age and growth rate	Wood cores extracted from five trees per stand, borer	246 cores
Needle retention	Number of years of needles retained	255 trees
Spruce sample collection—two sets	1st, 2nd and 3rd year of samples	765 samples
GER2600 spruce foliage spectra	Foliar reflectance spectra	765 samples
Lignin, cellulose and nitrogen levels	NIR spectroscopy	765 samples
Foliar chlorophyll and carotenoid levels	Laboratory extraction and analyses	765 samples

^aAirborne Solid-state Array Spectrometer (ASAS, NASA, Goddard Space Flight Centre).

^bField spectrometer GER2600 (Geophysical Environmental Research (GER) Corporation, Millbrook, New York).

^cThe brand names of the instruments used in the investigation are cited for descriptive purposes and are not intended to imply endorsement.

(acid-soluble compounds); and (4) lignin (Williams and Norris 1987, Martin 1994, ACCP 1994, Bolster *et al.* 1996). Foliar constituents were quantified as percentages of the initial sample weight; therefore the totals of foliar lignin, cellulose, polar and non-polar constituents sum to 100%.

2.5.2. Pigment analysis of fresh Norway spruce needles

First, second, and third year needles were separated from the branch at the study sites and placed directly into a portable freezing box (-4°C). Within 8 h of collection the samples were transported to a laboratory, weighed, and placed into a freezer, where they were stored at -70°C until analysis. The concentrations of chlorophylls *a* (Chl *a*) and *b* (Chl *b*) and the total amount of carotenoids ($C_{(x+c)}$) were determined spectrophotometrically. On average, 0.5 g of sampled frozen needles was placed in 10 ml of dimethylformamide (Porra *et al.* 1989) and left in the dark at 8°C for five days (120 h) until the needles were fully bleached. The absorbance of extracts was then measured at 480, 647 and 664 nm using a Unicam Helios α spectrophotometer (Unicam Ltd, Cambridge, UK), and pigment concentrations were calculated according to Wellburn (1994).

2.6. Airborne Solid-State Array Spectroradiometer (ASAS) data acquisition and processing

2.6.1. ASAS data acquisition

For this study, the Airborne Solid-state Array Spectroradiometer (ASAS) was flown onboard an Antonov AN-2 single engine biplane at an attitude of 2500 m, producing an 820 m swath-width with a $1.5\text{ m} \times 2.0\text{ m}$ nominal spatial resolution. Only nadir ASAS data were acquired. To minimize the effects of canopy shadow, the ASAS data were acquired as close to local solar noon as possible. A series of parallel, overlapping flight lines were flown at each of the three study areas S1-3 (figure 1). A detailed description of the data acquisition is available on the ASAS website at: <http://asas.gsfc.nasa.gov/browse/index.html>.

Due to weather restrictions, data acquisition occurred late in the summer of 1998, on 20 August and 1 September, between 10:30 am and 12:30 noon (Central European Time, or GMT +1 hour). The current-year spruce foliage was fully mature. Seventeen flight lines providing full coverage of the Krusne hory study areas were acquired. Due to the development of both high cirrus and low cumulus clouds around noon, only approximately 30% of the acquired ASAS data were of sufficient quality for further analyses. Although the flight lines were developed to cover the pre-selected study sites on the ground, only 23 (10 DC0, 5 DC1, 4 DC2, 4 DC3) of the 51 sampled sites were cloud-free.

2.6.2. ASAS sensor characteristics and data processing

The ASAS system is an airborne pushbroom imaging radiometer, with a 512×62 pixel CCD area array, maintained and operated by the Laboratory for Terrestrial Physics at the NASA Goddard Space Flight Centre (NASA, GSFC; Irons *et al.* 1991). The spectral range of ASAS covers 410–1032 nm, with a total of 62 narrow bands (9.5–11.5 nm at half-maximum, full width), and optimal spectral performance in the 450–900 nm region (Irons *et al.* 1991, Russell *et al.* 1997). Forty-five spectral bands were used to produce the imagery analysed in this study. Data were recorded as unsigned 16-bit digital numbers and calibrated to at-sensor

radiance using laboratory-derived sensor gain coefficients. Using hand-held solar photometers at the study areas during the overflights, the average aerosol optical thickness at 550 nm was determined to be 0.0502 for 20 August and 0.0475 for 1 September 1998. The Second Simulation of the Satellite Signal in the Solar Spectrum (6S) calibration model (US62 module with input conditions for the continental aerosol model) was applied to remove atmospheric effects and to convert the at sensor radiance to reflectance (Tanre *et al.* 1990).

Previous studies have established that forest canopy reflectance is anisotropic and therefore varies strongly as the directions and angle of solar illumination change (Kriebel 1978, Kimes *et al.* 1986, Ranson *et al.* 1991, Deering *et al.* 1994, Russell *et al.* 1997). For the current investigation, ASAS was flown consistently first over S1, then S2 and S3 (figure 1). The healthier forest stands were located on the westernmost slopes of the study area (S1) where data were acquired first (at approximately 11:00 am). The ASAS data over the more damaged stands to the east (S2 and S3) were acquired closer to local noon (when the ASAS view angle and the solar illumination angle were both closer to nadir). The sun therefore rose in elevation during the time for acquisition of all ASAS flight lines. Evaluating the ASAS imagery and the forest canopy and stand parameters in relationship to damage, it was established that a greater portion of the tree crowns were directly illuminated by the sun at the sites where data were acquired closer to noon. An increase in reflectance intensity, as solar elevation increases, due to the reduction of shadowing effects produced by the vertical structure of the vegetation canopies has been documented previously for coniferous stands and savannah (Kimes *et al.* 1986, Ranson *et al.* 1991, Deering *et al.* 1994, 1999). To account for the change in solar illumination a first order BRDF correction was applied (after Middleton 1992, Deering *et al.* 1994, 1999). Reflectance was computed as a product of the atmospherically corrected surface reflectance (extracted from the ASAS imagery) and the cosine of the solar zenith angle at the time of image acquisition, yielding reflectance at a standard zenith illumination angle.

Spectral reflectance data from both bright and dark ground targets (15 m \times 20 m lime and sand pits, and asphalt parking lots) were acquired using a GER2600 spectrometer simultaneously with the ASAS overflights for comparison with the reflectance spectra derived from ASAS. Validation of the ASAS calibration was conducted at GSFC during the summer of 1999. A vicarious hybrid calibration routine (Kovalick *et al.* 1994) was utilized that applied both the 6S code and the GER2600 measurements from ground reflectance targets (Dabney *et al.* 1999) to improve the retrieval of surface reflectance. In the spectral region 490–850 nm, ASAS and GER2600 reflectance data compared well for the bright lime target ($r=0.96$, reflectance range 30–53%), the ASAS measurements being 5–8% lower in magnitude. In the 450–490 nm and 850–900 nm regions, the lower ASAS values are likely caused by stray light contamination in the array affecting the radiometric calibration in the blue and portions of the near infrared, causing overcompensation for the radiation levels received in these spectral regions (Russell *et al.* 1997, Dabney *et al.* 1999).

2.6.3. Norway spruce canopy spectral extraction

The locations of the pre-selected 23 cloud-free field sites on the ASAS imagery (figure 2) were determined using 1:2500 colour infrared photography, 1:5000 scale forestry maps, and field surveys. The 1.5–2 m spatial resolution of the ASAS

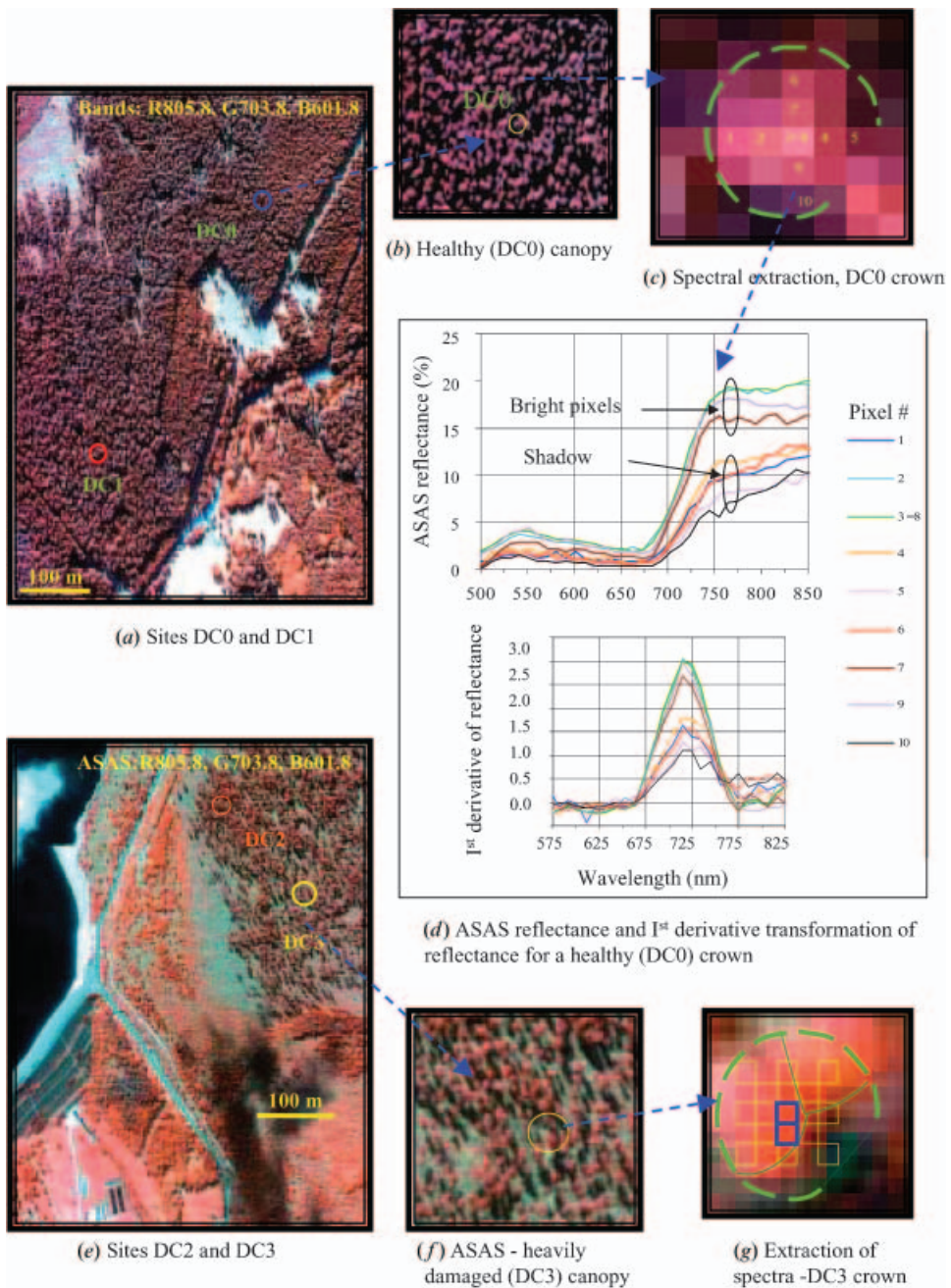


Figure 2. Extraction of reflectance spectra for Norway spruce canopies from individual tree crowns. Note the presence of heavier shadow within the canopy and the tree crowns of the healthy stand as compared to the severely damaged stand. The spectra used in the analyses were extracted from the brightest pixels within a tree crown (3c) and (3d) pixel 3=8 above; g—blue pixels). (a) Sites DC0 and DC1. (b) Healthy (DC0) canopy. (c) Spectral extraction, DC0 crown. (d) ASAS reflectance and first derivative transformation of reflectance for a healthy (DC0) crown. (e) Sites DC2 and DC3. (f) ASAS—heavily damaged (DC3) canopy. (g) Extraction of spectra—DC3 crown.

imagery allows for identification and selection of individual tree crowns from within the study sites (figure 2(b, f)). Reflectance data from 20–30 tree crowns per site were extracted to obtain spectra representative of the site's damage level.

An individual tree crown is represented in the imagery by 20–25 pixels (approximately 5×5 pixels; figure 2(c, g)). The spectral variation within a tree crown was evaluated by extracting spectral signatures from pixels along the orthogonal planes of the crown (figure 2(c)). The pixels on the sunlit side of a crown were relatively unaffected by shadowing. As the amount of shadow within a pixel increased, the noise within the spectra also increased (figure 2(d)). Individual tree canopy spectra were extracted from the brightest pixels, located on the sunlit portion of the crown, since they exhibited the least variation in reflectance data (figure 2(c, g)).

2.7. Data analyses

2.7.1. Spectral analyses

Applying a first order BRDF correction to the spectra, the effects of the solar zenith angle at the time of acquisition were minimized, but the absolute differences in canopy reflectance (base line shifts in reflectance magnitude, not spectral shifts) could be subject to a possible remaining effect of the changing solar zenith angle, altering the differences in magnitude. Spectral normalization, derivative transformation and band ratios/indices were used to assess the changes occurring in reflectance properties with increasing damage level, independently of the influence of the spectral amplitude variations.

2.7.1.1. Spectral properties of Norway spruce canopies by damage class. To determine the spectral regions optimal for damage detection, a sensitivity analysis of the canopy reflectance spectra was conducted following the procedure described by Carter *et al.* (1995). The sensitivity of the individual indices (SI) to the particular damage level i (table 3) was estimated by computing the relative change for each damage class (DC) from the healthy condition (Carter 1994), using the formula:

$$\text{SI to DC}i = (\text{IndexDC}i - \text{IndexDC}0) / \text{IndexDC}0. \quad (1)$$

To discriminate between overlapping bands and to determine if there are changes in the shape or position of the spectral features associated with the stand damage, a derivative analysis was conducted. The analysis is suggested as quantifying the possible effects of baseline shifts and removing scatter within the spectra (Miller *et al.* 1990, Martin 1994). The first derivative of reflectance was calculated using the formula:

$$D'_{\lambda i} = (R_{\lambda(i+1)} - R_{\lambda(i-1)}) / (\lambda_{(i+1)} - \lambda_{(i-1)}), \quad (2)$$

where $D'_{\lambda i}$ is the first derivative and $R_{\lambda i}$ is the mean reflectance value at wavelength λ_i .

2.7.1.2. ASAS spectral indices and their use in evaluation for separation of initial damage levels. Previous investigations have identified a wide range of spectral indices as indicators of vegetation physiological properties (Jordan 1969, Rock *et al.* 1986, 1988, Boochs *et al.* 1990, Chappelle *et al.* 1992, Gamon *et al.* 1992, 1997, Vogelmann *et al.* 1993, Carter 1994, Elvidge and Chen 1995, Fiella *et al.* 1996, Blackburn 1998, Datt 1998, Peñuelas 1998, Zarco-Tejada *et al.* 1999). The current

Table 3. Forest stand parameters, canopy pigments and chemical compounds tested for significant differences among damage levels¹.

Parameter	Damage level												DC groups
	DC 0—healthy			DC 1—initial			DC 2—intermediate			DC 3—heavy			
	Mean	SE	<i>n</i>	Mean	SE	<i>n</i>	Mean	SE	<i>n</i>	Mean	SE	<i>n</i>	
<i>1. Forest stand parameters</i>													
Tree height (m), $r=0.77^{**}$	22.54 ⁱ	0.48	77	19.28 ^j	0.52	67	18.75 ^j	0.51	68	16.77 ^k	0.69	38	3
DBH (cm), $r=0.79^{**}$	37.93 ⁱ	0.90	77	34.67 ^j	0.97	67	33.81 ^j	0.96	68	25.16 ^k	1.28	38	3
Age (years), $r=0.51^{*}$	62.69 ⁱ	2.30	70	50.00 ^j	2.40	65	52.07 ^j	2.38	66	48.40 ^j	2.90	43	2
Elevation (m), $r=0.71^{**}$	879.82 ^j	9.85	71	908.59 ⁱ	10.45	63	871.28 ^j	10.06	68	827.35 ^k	12.65	43	3
Years of needles retained (#), $r=0.82^{**}$	10.10 ⁱ	0.20	80	9.20 ^j	0.20	64	8.50 ^k	0.20	68	6.01 ^l	0.20	43	4
Canopy Closure (%), $r=0.71^{**}$	76.10 ⁱ	1.37	77	75.90 ⁱ	1.47	67	67.50 ^j	1.46	68	58.90 ^k	1.95	38	3
Total Basal Area (BA, m ² ha ⁻¹), $r=0.55^{*}$	28.22 ^{ji}	11.74	77	29.98 ⁱ	12.52	67	25.62 ^j	12.40	68	27.57 ^{ji}	16.70	38	2
Standard Density (trees ha ⁻¹), ns	25.00	1.50	77	26.99	1.61	67	24.06	1.60	68	28.63	2.14	38	—
<i>2. Photosynthetic pigments</i>													
Chlorophyll <i>a</i> (mg g ⁻¹ dw), $r=0.43^{*}$	2.81 ⁱ	0.05	78	2.78 ⁱ	0.062	67	2.49 ^j	0.06	68	2.44 ^j	0.08	38	2
Chlorophyll <i>b</i> (mg g ⁻¹ dw), $r=0.48^{*}$	0.99 ⁱ	0.02	77	0.97 ⁱ	0.023	67	0.86 ^j	0.02	68	0.83 ^j	0.03	38	2
Chlorophyll (<i>a+b</i>) (mg g ⁻¹ dw), $r=0.55^{*}$	3.79 ⁱ	0.07	70	3.75 ⁱ	0.084	65	3.35 ^j	0.08	66	3.29 ^j	0.10	43	2
Chl <i>a</i> / Chl <i>b</i> , $r=0.68^{**}$	2.85 ⁱ	0.01	71	2.89 ^j	0.012	63	2.92 ^k	0.01	68	2.96 ^l	0.01	43	4
Carotenoids (<i>Car</i>) (mg g ⁻¹ dw), $r=0.45^{*}$	0.47 ⁱ	0.01	80	0.46 ^{ij}	0.011	64	0.44 ^j	0.01	68	0.44 ^{ij}	0.01	43	2
Nitrogen (N) (mg g ⁻¹ dw), ns	1.43	0.01	77	1.43	0.009	67	1.42	0.01	68	1.41	0.01	38	—
Chl (<i>a+b</i>)/N, $r=0.50^{*}$	2.69 ^j	0.05	80	2.58 ⁱ	0.061	67	2.36 ^j	0.06	68	2.29 ^j	0.10	38	2
<i>Car</i> /N, $r=0.56^{*}$	0.34 ⁱ	0.01	77	0.32 ⁱ	0.008	67	0.31 ^j	0.01	68	0.31 ^j	0.01	43	2
<i>3. Foliar chemical compounds (canopy scale)</i>													
Cellulose (%), $r=0.78^{**}$	40.35 ⁱ	0.16	80	39.47 ⁱ	0.171	67	38.32 ^j	0.16	74	34.06 ^k	0.19	45	3
Polar (%), $r=0.77^{**}$	30.07 ⁱ	0.16	85	30.85 ⁱ	0.189	70	33.61 ^j	0.19	74	36.01 ^k	0.22	47	3
Non-polar (%), $r=0.89^{**}$	3.48 ⁱ	0.04	85	3.62 ^j	0.043	70	3.69 ^j	0.04	75	3.97 ^k	0.05	47	3

¹Statistically different parameter means ($p \leq 0.05$) are designated with different superscript lower-case letters.

^{**} $p \leq 0.01$, ^{*} $p \leq 0.05$.

study evaluated the potential of a number of the previously developed spectral indices and a few new ratios to determine which indices are best able to identify initial damage in Norway spruce stands (table 4). The spectral indices are organized according to their bandwidth, the regions they cover and the data treatment involved for their computation in the following groups: (1) high resolution indices—products of direct (simple) computation preserving the ASAS spectral resolution; (2) broadband indices (Landsat TM spectral bands and 15 nm wide bands) developed to assess the potential for stress detection of multispectral systems; (3) derivative indices; and (4) Inverted Gaussian Model (IGM) parameters. The computation of some of the more complex indices is described below.

- **Normalized red edge bands:** The ASAS spectra from the red edge region (680–735 nm) were normalized to minimum reflectance at 673 nm (where reflectance was minimum in the chlorophyll well) and a maximum reflectance at 744.5 nm (the last band before the oxygen absorption feature at 754–764 nm, figure 3(a)), minimizing the possibility for a baseline shift in spectra due to bi-directional effects. The potential for damage detection of the normalized spectral bands (N_{683} , N_{693} , N_{704} , N_{714} , N_{724} , N_{734} ; table 3) is compared to the remaining high spectral resolution indices.
- **Derivative indices:** D_{\max} is defined as the maximum value of the first derivative in the 675–740 nm region. The red edge inflection position ($\text{REIP}_{\text{wave}}$ —defined as the point of maximum slope of the red edge) was computed as the wavelength at which the first derivative data have maximum value (Horler *et al.* 1983, Rock *et al.* 1988). After applying the first derivative transformation to the extracted from the imagery spectra, the indices D_{\max}/D_{704} , D_{714}/D_{704} , D_{\max}/D_{714} and D_{\max}/D_{744} ($D_{\max} \equiv \text{REIP}_{\text{slope}}$) were calculated to assess the changes in the shape of the first derivative curve occurring with damage levels.
- **Inverted Gaussian model application:** Miller *et al.* (1990) demonstrated that the approximation of the red edge position from simple derivative analysis depends on instrument spectral resolution and suggest the use of the inverted Gaussian model (IGM) for obtaining red edge parameters. Using the IGM approach in the current study, the following parameters were generated: λ_o (wavelength at which the minimum reflectance in the chlorophyll absorption feature occurs), R_o (reflectance at λ_o), R_s (maximum reflectance in the NIR shoulder region—720–800 nm), λ_π (the wavelength at which the maximum of the first derivative of reflectance occurs, $\lambda_\pi = \text{REIP}_{\text{wave}}$) and σ ($\sigma = \lambda_\pi - \lambda_o$). An inverted Gaussian curve was fitted to the data using the equation:

$$R_\lambda = R_s - \left((R_s - R_o) \exp \left(-(\lambda_o - \lambda_\pi)^2 / 2\sigma^2 \right) \right).$$

The IGM was applied using the nonlinear least squares mathematical procedure and 14 ASAS bands from the 673–805 nm region. The IGM requires an initial estimation of the parameters of the model done by careful analysis of the spectra (Miller *et al.* 1990) for representation of the red edge. In the current study, the starting IGM parameters were $\lambda_o = 673$ nm, $R_o = 5\%$, $\sigma = 40$ nm and $R_s = 40\%$.

2.7.2. Statistical analyses

The significance level of the differences among ASAS reflectance and derivative spectra at each wavelength per damage level was determined by analysis of

Table 4. High-resolution band ratios and normalized bands, computed using ASAS reflectance spectra. Their potential for stress detection is evaluated based on indices sensitivity to damage level and statistical significance of the differences among damage level means¹ (ANOVA, $n = 23$).

		Index sensitivity			Damage levels (ANOVA means and standard errors)									
Index ²	Algorithm	DC1	DC2	DC3	DC0	DC1	DC2	DC3	<i>r</i>	DC groups				
High (10 nm) resolution band ratios														
C ₁	R_{693}/R_{775}^3	0.13	0.70	1.06	0.16 ⁱ	0.003	0.19 ^j	0.005	0.28 ^k	0.008	0.34 ^l	0.006	$r = 0.97^{**}$	4
C ₂	R_{693}/R_{500}	—	—	—	2.62	0.095	2.41	0.055	2.09	0.035	2.22	0.043	ns	—
V ₁	$R_{744.5}/R_{724}$	−0.03	−0.17	−0.22	1.59 ⁱ	0.005	1.55 ^j	0.014	1.33 ^k	0.017	1.25 ^l	0.009	$r = 0.87^{**}$	4
V ₂	$(R_{731} - R_{724})/(R_{731} + R_{724})$	−0.06	−0.55	−0.68	−0.10 ⁱ	0.001	−0.09 ⁱ	0.003	−0.04 ^j	0.004	−0.03 ^j	0.002	$r = 0.81^{**}$	2
V ₃	$(R_{734.2} - R_{744.5})/(R_{714} + R_{724})$	−0.07	−0.57	−0.71	−0.12 ⁱ	0.002	−0.11 ⁱ	0.004	−0.05 ^j	0.005	−0.03 ^k	0.002	$r = 0.80^{**}$	3
PRI ₁	$(R_{531.8} - R_{571})/(R_{531.8} + R_{571})$	0.10	−0.64	−0.87	0.10 ⁱ	0.003	0.12 ⁱ	0.004	0.04 ^j	0.004	0.01 ^k	0.003	$r = 0.73^{**}$	3
PRI ₂	$(R_{551.5} - R_{531.8})/(R_{551.8} + R_{531.8})$	—	—	—	0.03	0.003	0.01	0.004	0.03	0.002	0.03	0.002	ns	—
PRI ₃	$(R_{571} - R_{541.8})/(R_{571} + R_{541.8})$	0.02	−0.50	−0.74	−0.13 ⁱ	0.003	−0.13 ⁱ	0.004	−0.06 ^j	0.004	−0.03 ^k	0.003	$r = 0.78^{**}$	3
RE ₁	Average ($R_{673} \dots R_{703.8}$)	0.13	1.20	1.88	3.59 ⁱ	0.035	4.05 ^j	0.176	7.88 ^k	0.300	10.34 ^l	0.259	$r = 0.98^{**}$	4
RE ₂	Average ($R_{714} \dots R_{724}$)	0.06	0.56	0.84	11.63 ⁱ	0.090	12.36 ^j	0.334	18.08 ^k	0.476	21.34 ^l	0.441	$r = 0.95^{**}$	4
RE ₃	Average ($R_{734.2} \dots R_{744.5}$)	0.01	0.26	0.43	19.83 ⁱ	0.142	19.97 ⁱ	0.307	25.06 ^j	0.467	28.27 ^k	0.505	$r = 0.86^{**}$	3
SR	$R_{744.5}/R_{673}$	−0.02	−0.46	−0.65	12.11 ⁱ	0.122	11.88 ⁱ	0.209	6.59 ^j	0.325	4.24 ^k	0.101	$r = 0.93^{**}$	3
SIPI	$(R_{795.5} - R_{502.2})/(R_{795} - R_{642.5})$	−0.01	0.03	0.08	1.02 ⁱ	0.001	1.01 ⁱ	0.002	1.05 ^j	0.004	1.10 ^k	0.005	$r = 0.84^{**}$	3
RARS _a	$R_{673}/R_{703.8}$	−0.02	0.47	0.74	0.26 ^j	0.002	0.26 ⁱ	0.003	0.38 ^j	0.010	0.46 ^k	0.006	$r = 0.99^{**}$	3
RARS _b	$R_{673}/(R_{652.5} \times R_{703.9})$	−0.01	−0.37	−0.53	0.13 ⁱ	0.001	0.13 ⁱ	0.003	0.08 ^j	0.004	0.06 ^k	0.002	$r = 0.83^{**}$	3
RARS _c	$R_{775}/R_{502.2}$	−0.15	−0.49	−0.61	16.02 ⁱ	0.548	13.68 ^j	0.317	8.17 ^k	0.404	6.18 ^l	0.188	$r = 0.62^*$	4
PSSR _a	$(R_{795.5} - R_{683.2})/(R_{795} + R_{683.2})$	−0.02	−0.18	−0.28	0.83 ⁱ	0.001	0.82 ⁱ	0.006	0.68 ^j	0.011	0.60 ^k	0.007	$r = 0.97^{**}$	3
PSSR _b	$(R_{795.5} - R_{601.8})/(R_{795} + R_{601.8})$	−0.02	−0.14	−0.17	0.77 ⁱ	0.002	0.76 ⁱ	0.003	0.63 ^j	0.009	0.58 ^k	0.007	$r = 0.98^{**}$	3
PSSR _c	$(R_{795.5} - R_{502.2})/(R_{795} + R_{502.2})$	−0.02	−0.14	−0.17	0.87 ⁱ	0.002	0.85 ⁱ	0.004	0.75 ^j	0.009	0.72 ^k	0.006	$r = 0.95^{**}$	3
Normalized bands														
N ₆₈₃ ⁴	$((R_{683} - R_{670})/(R_{744.5} - R_{670})) \times 100$	0.37	0.57	1.01	4.02 ⁱ	0.08	5.53 ^j	0.39	6.30 ^k	0.26	8.08 ^l	0.24	$r = 0.46^*$	4
N ₆₉₃	$((R_{693} - R_{670})/(R_{744.5} - R_{670})) \times 100$	0.18	0.36	0.54	12.43 ⁱ	0.10	14.64 ^j	0.61	16.85 ^k	0.37	19.17 ^l	0.28	$r = 0.53^{**}$	4
N ₇₀₄ ⁵	$((R_{704} - R_{670})/(R_{744.5} - R_{670})) \times 100$	0.12	0.33	0.46	25.10 ⁱ	0.15	28.02 ^j	0.77	33.28 ^k	0.61	36.54 ^l	0.44	$r = 0.62^{**}$	4
N ₇₁₄	$((R_{714} - R_{670})/(R_{744.5} - R_{670})) \times 100$	0.08	0.24	0.31	41.84 ⁱ	0.19	45.00 ^j	0.89	52.00 ^k	0.72	54.73 ^l	0.43	$r = 0.68^{**}$	4
N ₇₂₄	$((R_{724} - R_{670})/(R_{744.5} - R_{670})) \times 100$	0.03	0.13	0.17	63.14 ⁱ	0.16	65.18 ^j	0.65	71.58 ^k	0.63	73.93 ^l	0.39	$r = 0.62^{**}$	4
N ₇₃₄	$((R_{734} - R_{670})/(R_{744.5} - R_{670})) \times 100$	0.02	0.07	0.09	79.13 ⁱ	0.12	81.00 ^j	0.53	84.70 ^k	0.47	86.42 ^l	0.27	$r = 0.59^{**}$	4

^{**} $p \leq 0.01$, ^{*} $p \leq 0.05$.

¹Statistically different index means ($p \leq 0.05$) per damage class are designated with different superscript lower-case letters.

²The indices are adjusted to the ASAS band centres (listed in the algorithm in subscript); references are listed in the Methods section of the paper.

³ R_{λ} : R reflectance (%).

⁴ N_{λ} : N normalized reflectance.

⁵The indices offering highest potential for RS separation of the initial damage (DC1) are in bold.

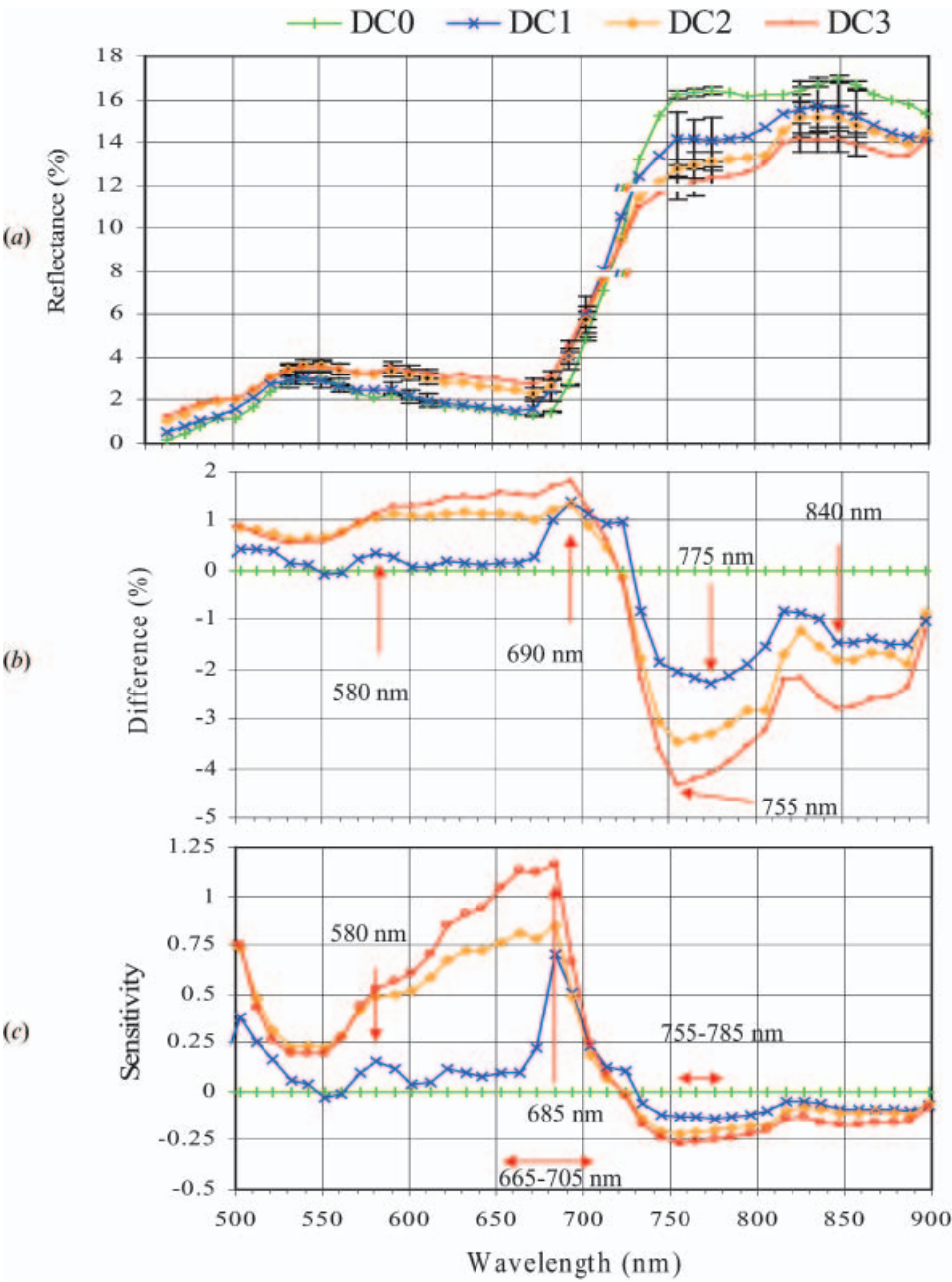


Figure 3. Reflectance (a) and sensitivity to damage of Norway spruce forest canopy (least square means \pm SE, ANOVA). Reflectance difference (b) was computed by subtracting mean reflectance of healthy canopy from that of damaged canopy. Reflectance sensitivity to damage (c) was computed by dividing the reflectance difference by mean reflectance of the non-stressed canopy. The red arrows in (b) indicate the maximal differences and in (c) indicate the regions for which differences between DC0 and DC1 were significant, according to ANOVA and the Tukey–Kramer test.

variances (ANOVA) and Tukey–Kramer pair-wise mean comparisons test (SYSTAT 7.0, SPSS Inc. 1997). The relationships between spectral indices and foliar constituents (chemistry, pigments) and between spectral indices and forest stand parameters were evaluated using simple correlation analysis (Zar, 1996). For the spectral indices, statistically significant differences between damage classes were determined using ANOVA. The significance of the differences was determined using the Tukey–Kramer test.

3. Results and discussion

3.1. Differences in forest bio-physiological parameters in relation to damage level

3.1.1. Changes in forest stand parameters associated with damage

The forest stand parameters, age, canopy closure, number of needle age classes retained and elevation, differed significantly with damage level (table 3). The most reliable field indicator of damage was the number of needle age classes retained ($r=0.82$, $p\leq 0.01$), which declined as the damage increased. Linear reductions were also observed for DBH ($r=0.79$, $p\leq 0.01$), tree height ($r=0.77$, $p\leq 0.01$) and canopy closure ($r=0.71$, $p\leq 0.01$) (table 3). The more heavily damaged stands were located at the lower elevations and were of relatively younger age. Their canopies were significantly more open (lower canopy closure), thus producing proportionally less shadow (table 3; figure 3(a, e)). Canopy spectral properties are typically controlled by canopy density, structural and optical properties and leaf area index (Dickinson 1984). The present findings demonstrate the importance for remote sensing of forest health to detect the changes in foliar amount and properties occurring with advancing damage.

The occurrence of more heavily damaged forest stands at the lower elevations, established by this study, is in contrast with the previously reported trend for broad elevational ranges (601–800 m and 801–1000 m) of severe forest damage occurring at the higher elevations in the Krusne hory (Rock *et al.* 1993, Ardo *et al.* 1997, Lambert *et al.* 1995). Within the small (approximately 100 m) elevational gradient of this study, the variation of forest damage observed with elevation could be explained by the longer retention of air-pollution masses at the lower elevation, where the trees were more protected from the winds, and most likely by the closer proximity to the pollution sources of some of the lower elevation sites. By the time the pollution levels in the Krusne hory reached damaging levels, which have been reported since 1965 (Kubikova 1991), the older forests may have been better established and less susceptible to the air pollution damage than the younger forests which suffered greater damage and higher mortality. The lower canopy closure of the more damaged sites was caused by crown defoliation and thinning and was not associated with significant differences in the forest stand density (table 3).

3.1.2. Differences in foliar pigment levels associated with forest damage

Pigment levels (i.e. Chl *a*, Chl *b* and carotenoids) were relatively stable across damage levels. However, significant differences in the Chl *a/b* ratio occurred with increasing damage level, identifying this ratio as a sensitive bio-indicator of damage in the Krusne hory (table 3).

Previous investigations have demonstrated a strong relationship between vegetation stress and foliar pigment levels, considering pigments among the most sensitive indicators of plant stress (Rock *et al.* 1986, Lichtenthaler 1988). The majority of those investigations have studied the changes in foliar pigment levels

shortly after introducing a stress agent to the vegetation grown under otherwise optimal conditions. However, this study addressed the long-term effect of the stress factors in the Czech Republic (SO_2 air pollution was reported since the 1950s, maximum severity in the 1960s–1970s) followed by a recovery during the period 1980–1995 (Entcheva *et al.* 1996), explaining the relatively stable pigment levels across the study areas. In addition, the forest damage classes used in this study represent a combination of stand and individual tree parameters. Therefore, depending on the degree of canopy closure, two stands can have a very different foliar pigment concentration per unit of canopy area, while the pigment concentration per unit of leaf mass could be similar. This complexity could account as well for the lack of a strong correlation between damage level and photosynthetic pigments.

3.1.3. *Changes in foliar constituents associated with forest damage level*

A strong change in the balance of foliar constituents occurred with increasing damage level (table 3). At the more severely damaged stands, the amount of structural compounds (foliar lignification and cellulose content) was significantly lower, while the remaining chemical compounds (polar and non-polar) were at proportionally higher levels. The strongest association with damage was shown for the non-polar constituents (increasing with damage; $r=0.89$, $p\leq 0.01$; fats, waxes—organic soluble compounds) for which the initial damage was evident and for the polar compounds ($r=0.77$, $p\leq 0.01$; water soluble). The remaining foliar compounds, cellulose ($r=0.78$, $p\leq 0.01$) and lignin ($r=0.70$, $p\leq 0.01$), were strongly negatively associated with damage level (table 3). Since lignin, cellulose, polar and non-polar compounds were determined by a carbon fractionation analysis as a proportion of the sample's dry weight, the strong relationships established among all four constituents were anticipated (Newman *et al.* 1994). This study demonstrates that changes in the balance of foliar chemical constituents, such as the decrease in lignification and increase in non-polar compounds established here, occur in association with forest damage and can serve as sensitive indicators of change in the forest physiological condition due to long-term stress. Therefore, remote sensing based on spectral foliar canopy chemistry estimates can provide a sensitive approach for evaluation of forest health.

3.2. *Canopy reflectance properties*

3.2.1. *Norway spruce canopy reflectance properties*

In the visible and red-edge region, higher canopy reflectance intensity was detected by ASAS from the more heavily damaged canopies, while in the near infrared the opposite spectral trend was evident: the healthy (DC0) stands had the highest NIR reflectance (figure 3(a)). The shapes of the spectral curves by damage level confirmed the spectral trends reported by earlier studies for spruce using foliar and canopy spectra (Rock *et al.* 1988, Ekstrand 1996, Entcheva *et al.* 1996, Entcheva 2000). The standard deviations of the data around the means were higher for damaged forests as compared to healthy stands ($\text{SD}_{\text{DC3}} > \text{SD}_{\text{DC2}} > \text{SD}_{\text{DC1}}$). The variation of the data around the means for DC0 and DC1 was maximum around 685 nm, while for DC2 and DC3 the variation was greatest at lower wavelengths (673 nm and 642 nm, respectively).

Reflectance difference peaks (figure 3(b)) occurred in the 680–720 nm and 740–810 nm regions, with maxima at 690 nm, 755–775 nm and 840 nm for all damage levels. Based on ANOVA and Tukey–Kramer tests performed at each

band, the differences among the means across all damage levels were statistically significant ($p < 0.01$) at 580 nm and in the red edge (675–705 nm) and NIR (755–785 nm) regions (figure 3(b)). The sensitivity peaks (figure 3(c)) for DC1 were located in the 695–720 nm range, while for DC2 and DC3 the peaks were in the broader 580–705 nm range. For all damage levels, the sensitivity maximum occurred at 685 nm (figure 3(c)). Although differences in the 730–900 nm region were large (figure 3(b)), the sensitivity to damage of this region was low (figure 3(c)), suggesting a low potential for spectral damage separation. The spectral analysis indicates that *the 670–705 nm region (685 nm maximum) has the highest potential for initial damage level separation* in Norway spruce canopies. Therefore, RS using ratios of narrow bands (< 20 nm), a band from the sensitive region (670–705 nm, optimally 685 nm) and a band from the regions with lower sensitivity (such as the NIR), provide potential for forest health assessment and detection of early vegetation stress.

3.2.2. Canopy reflectance properties of normalized reflectance spectra

Normalizing the ASAS reflectance to a minimum at 675 nm and a maximum at 745 nm allowed an evaluation of the reflectance properties in the red edge region, independently of the influence of the spectral amplitude variation. In the red edge region (figure 4), reflectance increased significantly with damage throughout the 685–735 nm region, and was maximal around the middle of this spectral region—at 705 nm and 715 nm. The higher reflectance in the 670–710 nm region observed with increasing damage level is a typical spectral response of vegetation under stress (Rock *et al.* 1986, 1988). The normalization approach allows the red edge properties to be used for separation of damage classes based on physiological differences occurring with damage (e.g. decrease in chlorophyll levels) rather than canopy

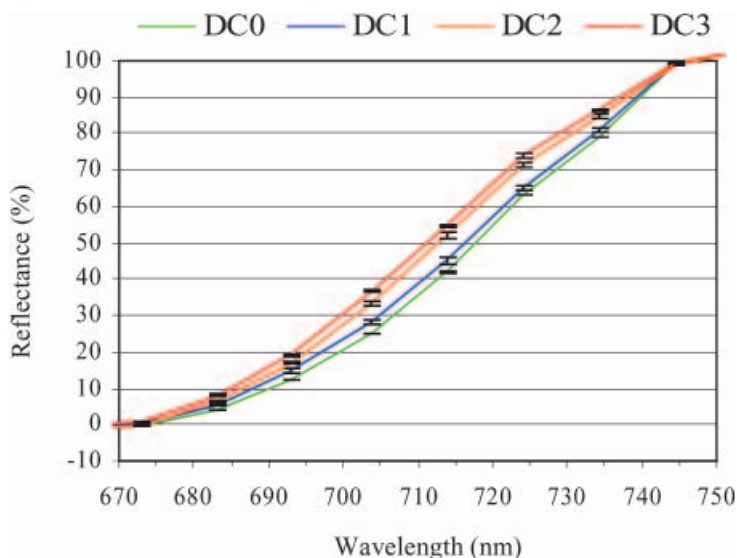


Figure 4. Normalized ASAS reflectance (least square means \pm SE). To evaluate reflectance properties in the red edge region ASAS reflectance spectra were normalised to 670 nm (minimum = 0%) and 744 nm (maximum = 100%) wavelengths.

structural and morphological changes. The sensitivity of the 705–715 nm normalized bands to damage level is discussed below with the computed spectral indices.

3.2.3. Derivative analysis

Using a derivative analysis, the pattern and location of the Norway spruce reflectance spectral features was determined for each damage level, which revealed significant differences among damage levels. The first derivative in the 675–745 nm (the red edge) region for healthy forest (DC0) was characterized with a narrow peak, when, for the damaged forests, the peaks were considerably broader (figure 5). The peaks for DC0 and DC2 were centred at around 725 nm, while for DC1 and DC3 they were centred at 715 nm. *With increase in damage, a shift of the red edge reflectance curve toward shorter wavelengths was seen.* In previous field studies, the shift of the derivative maxima in the 685–745 nm region (see REIP_{wave}, figure 5) has been attributed to a decrease in Chl *a* and Chl *b* concentrations with increased damage. A second peak in the derivative spectra occurred for DC 0 at 840 nm, for DC1 at 810 nm, for DC2 at 815 nm and for DC3 at 805 nm (figure 5). A damage associated change in the shape of the reflectance curve was observed in the NIR region, ranging from a nearly level curve for the healthy stands to more pronounced peaks with increasing damage.

With increasing damage level, the variation of the data around the means increased, with the least amount of overlap among standard deviations present in the red edge region. *Statistically significant differences in the derivative spectra with damage class occurred in the 685–740 nm and 780–840 nm regions ($p < 0.01$).* There were statistically significant differences between healthy canopies and the intermediate and advanced damage at 815 nm ($p < 0.01$) and between healthy and initial damage at 830 nm ($p < 0.05$). In the present study, there was no significant difference in the position of the derivative maximum REIP_{wave} between DC0 and DC1, but there was a significant difference between DC0 and DC2 and DC3 as a group (figure 5).

Although the spectral resolution of ASAS (10 nm) proved to be marginal for conducting derivative analysis, the regions of spectral shifts and differences magnitudes were established. Therefore, ratios of a band from these regions

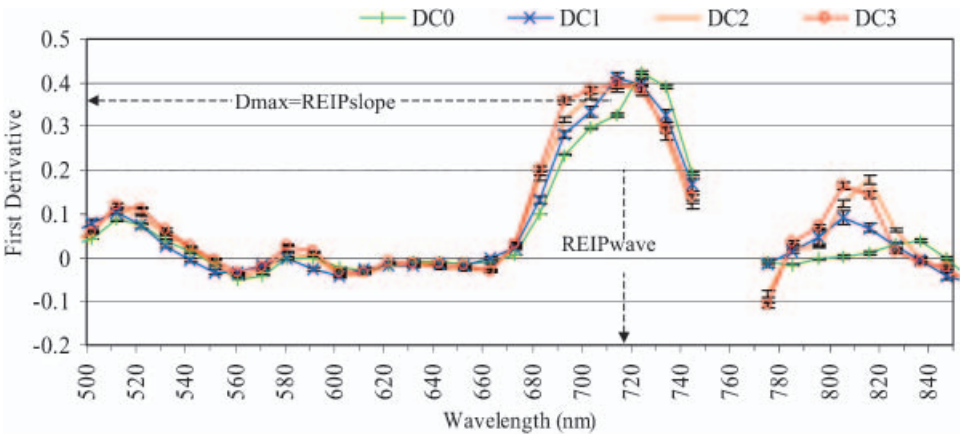


Figure 5. First derivative transformation of ASAS reflectance spectra (least square means \pm SE).

(optimally 720–725 nm) to a band from the spectra less sensitive to damage provide potential for RS detection of early changes in forest health, independently of the effects of baseline shifts and scatter on the spectra.

3.3. Evaluation of ASAS spectral indices for separation of initial damage levels

This study evaluated the use of high spectral resolution data for separation of damage levels in Norway spruce canopy using a wide range of algorithms (tables 4 and 5). The coefficients of determination of the spectral indices to damage severity and the sensitivity of a particular index to individual damage level were used as an indicator for evaluating the detection potential of the algorithms. Seven spectral indices were identified as having the highest potential for separation of the initial damage level (DC1) from healthy stands (DC0) (figure 6). These are organized into five major groups: (1) high (10 nm) resolution band ratios, (2) high resolution normalized bands, (3) broadband indices (Landsat TM and 15 nm bands), (4) high resolution derivative indices, and (5) inverted Gaussian model (IGM) parameters (tables 4 and 5).

3.3.1. Optical indices (simple band ratios)

The C_1 index (Carter 1994) generates a ratio of reflectance at 695 nm (strongly sensitive to changes in chlorophyll concentration) and the NIR at 775 nm (sensitive to biomass and insensitive to pigments) (figure 6(a)). This ratio was modified for use with ASAS, using band 29 centred at 695 nm to band 37 centred at 775 nm. This ratio increased with increasing damage and differed significantly for healthy canopies as compared to DC1, DC2 and D3 ($r^2=0.93$) (table 4). The sensitivity of the index to damage was relatively strong, as compared to the remaining indices ($C_{DC1}=0.13$) (table 4).

The RE_1 index, the average amount of reflectance in the 673–703.8 nm region (Vogelmann *et al.* 1993), shows high sensitivity to all damage levels (figure 6(a)). The index is strongly correlated to damage ($r^2=0.96$) and its sensitivity to DC1 is relatively high ($RE1_{DC1}=0.13$) (table 4).

The pigment specific indices $RARS_a$ (R_{675}/R_{705} , $r^2=0.97$), $RARS_b$ (using reflectance at 673, 652.5 and 703.9 nm; $r^2=0.70$) and $RARS_c$ (R_{775}/R_{500} ; $r^2=0.38$), suggested as strongly sensitive to changes in pigment levels (Chappelle *et al.* 1992), display relatively higher sensitivity to DC2 and DC3 when ranked among the other indices. However, only $RARS_c$ has a high sensitivity to DC1 ($RARS_c_{DC1}=-0.15$) (table 4, figure 6(a)).

A comparison among all high-resolution band ratios (table 4) suggests a high potential for separation of initial damage (DC1) when using either of the C_1 , RE_1 or $RARS_c$ spectral indices.

The photochemical indices PRI_1 (using reflectance at 530 and 570 nm) and PRI_3 (at 540 and 570 nm), which, it has been suggested (Fiella *et al.* 1996, Gamon *et al.* 1997), are strongly related to leaf physiological state and photosynthetic radiation use efficiency, were sensitive to the intermediate and advanced damage levels but were not able to separate the initial DC1 damage (table 4).

3.3.2. Normalized red edge bands

Reflectance for the normalized bands increased with increasing damage level (figure 4). There were statistically significant differences among normalized spectra

Table 5. Spectral derivative and broadband indices and IGM parameters. The indices were computed using ASAS reflectance spectra. Their potential for stress detection is evaluated based on index sensitivity to damage level and statistical significance of the differences among damage level means¹ (ANOVA, $n = 23$).

Index ²	Algorithm	Index sensitivity			Damage levels (ANOVA means and standard errors)								DC groups	
		DC1	DC2	DC3	DC0		DC1		DC2		DC3			<i>r</i>
<i>Broadband indices (Landsat TM and 15 nm)</i>														
NDVI	$(R_{795.5}-R_{673})/(R_{795}+R_{673})$	-0.01	-0.17	-0.26	0.86 ⁱ	0.01	0.86 ⁱ	0.01	0.71 ^j	0.01	0.63 ^k	0.01	$r=0.99^{**}$	3
TVI	$(^d\sqrt{\text{NDVI}})\times 100$	0.00	-0.05	-0.09	116.40 ⁱ	0.05	116.40 ⁱ	0.05	110.01 ^j	0.47	106.39 ^k	0.35	$r=0.99^{**}$	3
R_{550}/R_{700} ³	$R_{551.5}/R_{703.8}$	—	—	—	0.61	0.01	0.60	0.01	0.63	0.01	0.58	0.01	ns	—
R_{850}/R_{700}	$R_{857.5}/R_{693}$	-0.03	-0.33	-0.51	6.37 ⁱ	0.09	6.16 ⁱ	0.15	4.29 ^j	0.17	3.12 ^k	0.05	$r=0.67^*$	3
R_{850}/R_{550}	$R_{857.5}/R_{551.5}$	0.01	-0.22	-0.30	5.77 ⁱ	0.05	5.82 ⁱ	0.07	4.50 ^j	0.12	4.06 ^k	0.09	$r=0.81^{**}$	3
R_{815}/R_{740}	$R_{816.2}/R_{744.5}$	0.03	0.12	0.13	1.06 ⁱ	0.00	1.10 ^j	0.01	1.19 ^k	0.01	1.20 ^k	0.01	$r=0.77^{**}$	3
R_{734}/R_{693}	$R_{744.6}/R_{693}$	-0.05	-0.36	-0.50	4.98 ⁱ	0.04	4.72 ^j	0.08	3.21 ^k	0.10	2.47 ^l	0.04	$r=0.86^{**}$	4
R_{734}/R_{714}	$R_{744.6}/R_{714}$	-0.03	-0.17	-0.23	1.86 ⁱ	0.01	1.81 ⁱ	0.01	1.55 ^j	0.02	1.43 ^k	0.01	$r=0.96^{**}$	3
R_{550}/R_{600}	$R_{551.5}/R_{601.8}$	-0.01	-0.18	-0.27	1.43 ⁱ	0.01	1.41 ⁱ	0.01	1.18 ^j	0.01	1.05 ^k	0.01	$r=0.85^{**}$	3
<i>Derivative indices</i>														
REIP _{wave}	Position of D^4 maximum (670–730 nm)	-0.01	-0.03	-0.02	725.26 ⁱ	0.23	724.51 ⁱ	0.46	719.97 ^j	0.65	716.84 ^k	1.41	$r=0.85^{**}$	3
REIP _{slope} ⁵	REIP _{slope} = D_{max} (670–730 nm region)	-0.02	-0.06	-0.09	0.43 ⁱ	0.01	0.42 ^{ij}	0.01	0.40 ^{ji}	0.01	0.39 ^j	0.01	$r=0.84^{**}$	2
D_{714}/D_{704}	$D_{714}/D_{703.8}$	-0.06	-0.27	-0.33	1.31 ⁱ	0.01	1.24 ^j	0.02	0.95 ^k	0.02	0.88 ^l	0.02	$r=0.95^{**}$	4
D_{max}/D_{714}	D_{max}/D_{714}	-0.03	-0.15	-0.20	1.32 ⁱ	0.01	1.29 ^j	0.01	1.12 ^j	0.01	1.05 ^k	0.01	$r=0.92^{**}$	3
D_{max}/D_{704}	$D_{\text{max}}/D_{703.8}$	-0.10	-0.14	-0.15	1.47 ⁱ	0.02	1.32 ^j	0.03	1.26 ^k	0.03	1.25 ^k	0.08	$r=0.79^{**}$	3
D_{max}/D_{744}	$D_{\text{max}}/D_{744.5}$	0.05	0.74	0.60	2.67 ⁱ	0.10	2.79 ⁱ	0.12	4.64 ^j	0.30	4.27 ^j	0.33	$r=0.71^{**}$	2
<i>Inverted Gaussian model (IGM) parameters</i>														
R_s	R maximum (670–850 nm region), IGF	0.06	0.36	0.51	22.74 ⁱ	0.17	24.13 ^j	0.38	30.99 ^k	0.53	34.26 ^l	0.58	$r=0.81^{**}$	4
R_o	R minimum (670–850 nm region), IGF	0.59	7.09	10.63	0.55 ⁱ	0.02	0.88 ^j	0.09	4.47 ^k	0.24	6.42 ^l	0.21	$r=0.96^{**}$	4
λ_o	Wavelength position of R_o , IGF	-0.02	-0.01	-0.01	671.80 ⁱ	0.10	670.45 ^j	0.29	666.08 ^k	0.46	664.00 ^l	0.84	$r=0.76^{**}$	4
σ	$(\lambda_o-\lambda_\pi)$, IGF	0.05	0.19	0.22	36.99 ⁱ	0.18	38.67 ^j	0.31	43.92 ^k	0.53	45.25 ^k	1.04	$r=0.67^*$	3
λ_π	Wavelength position of D_{max} , IGF	—	—	—	710.54	0.17	710.00	0.39	709.25	0.29	708.8	0.32	ns	—

$^{**}p \leq 0.01$, $^*p \leq 0.05$.

¹Statistically significant index means ($p \leq 0.05$) per damage level are designated with different superscript lower-case letters.

²The indices are adjusted to the ASAS band centres (listed in the algorithm in subscript); references are listed in the methods section of the paper.

³ R_λ : R reflectance (%).

⁴ D_λ : D derivative value, product of first derivative transformation of reflectance.

⁵The indices offering highest potential for RS separation of the initial damage (DC1) are in bold.

throughout the 683.2–734 nm region (table 4), but separation of healthy (DC0) from DC1, DC2 and DC3 was only possible using bands 704 nm and 714 nm. It is important to note that the normalized bands showed a relatively high sensitivity to initial damage (DC1), while their sensitivity to DC2 and DC3 was lower, as compared to R_o , RE_1 and C_1 (tables 4 and 5).

3.3.3. Landsat TM and broadband ratios

There was a strong correlation between the NDVI ($r^2=0.97$) and TVI ($r^2=0.98$) indices and damage class (table 5). The indices decreased in association with increasing damage level. While there were highly significant differences among means from DC2, DC3 and the combined group of DC0 and DC1, the differences

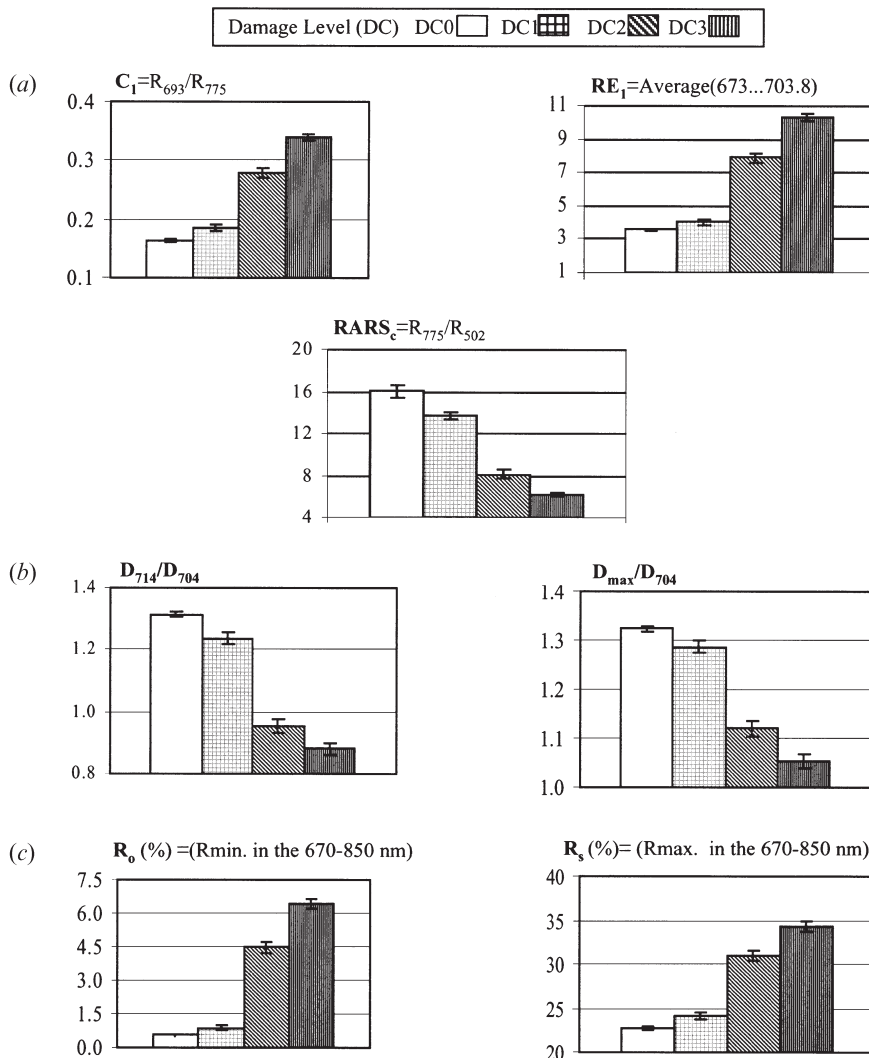


Figure 6. Canopy spectral reflectance indices with highest potential for separation of initial damage level, e.g. separation of DC1 from the remaining damage levels (least square means \pm SE).

between means from DC0 and DC1 were not significant. The results demonstrate the low potential of broadband multi-spectral systems for detection of the initial levels of damage.

3.3.4. Derivative indices

There has been little attention to the changes associated with damage in the magnitude of the first derivative ($REIP_{\text{slope}} = D_{\text{max}}$). Based on ANOVA results, there were highly significant differences in the $REIP_{\text{slope}}$ between DC0 and (DC1, DC2) and DC3 (table 5), with D_{max} decreasing for more advanced damage classes. While most of the computed derivative indices decreased in value with an increase in damage level, the D_{max}/D_{744} increased with an increase in damage level (table 5). The derivative indices D_{max}/D_{704} (figure 6(b)) and D_{714}/D_{744} (Vogelmann *et al.* 1993) had the highest sensitivity when ranked among the other derivative indices. The D_{max}/D_{704} , D_{max}/D_{714} and D_{714}/D_{704} ratios show statistically significant differences among all damage levels, while D_{max}/D_{744} is able to separate the combined group of DC2 and DC3 from the combined group of DC0 and DC1 (table 5). These results indicate the high potential for separation of the early stages of damage using the derivative indices D_{max}/D_{704} , D_{max}/D_{714} and D_{714}/D_{704} , with the D_{max}/D_{704} having the highest sensitivity to DC1.

3.3.5. Inverted Gaussian model (IGM) parameters

From the IGM parameters, the R_o (chlorophyll well) and R_s (NIR reflectance shoulder) indices had the highest relationship to the decline for all damage levels (table 5). The R_o increased significantly with increasing damage level (figure 6(c)). The R_o index sensitivity to initial damage (DC1) is 0.59, 7.09 to DC2 and 10.63 to DC3, suggesting a high potential of this index for separation of initial levels of stress as well as of intermediate and heavy damage. These results identify R_o as having the highest sensitivity and potential for separation of initial damage level among all of the evaluated spectral indices (tables 4 and 5).

3.3.6. Spectral indices: potential for RS assessment of forest health and separation of initial damage level

Evaluating the sensitivity and correlation of the indices from the different groups, the highest potential for RS separation of initial damage levels was demonstrated by R_o , followed by C_1 , RE_1 , N_{704} , D_{max}/D_{704} and the $RARS_c$ index. A comparison between the capabilities of broadband and high spectral resolution indices demonstrates the superior abilities of hyperspectral data for forest health monitoring and damage level separation.

3.4. Evaluation of the relationships between reflectance indices and foliar constituents

Reflectance properties at the canopy level are a function of canopy structure (e.g. stand density, canopy closure, canopy architecture, etc.) and forest biophysiological parameters that begin at the branch and leaf level (e.g. foliar pigment concentrations and chemical constituents such as lignin, cellulose and starch content). The strongest correlation revealed between the spectral indices and a canopy biophysical parameter was to non-polar foliar compounds (such as waxes, fats and oils): RE_1 ($r=0.88$), R_o ($r=0.87$), C_1 ($r=0.84$), N_{704} ($r=0.71$), R_s ($r=0.73$)

and D_{\max}/D_{704} ($r = -0.69$) (table 6). A number of spectral indices were also correlated with the level of lignin compounds: C_1 ($r = -0.69$), R_o ($r = -0.67$), RE_1 ($r = -0.66$), N_{704} ($r = -0.61$). Since foliar lignin and non-polar compounds do not have strong absorption features in the visible spectral region, the strong correlation between these compounds and the spectral indices is most likely due to the association of the foliar compounds with cell and leaf structure. A relatively high correlation to polar compounds (water-soluble compounds such as tannins) was exhibited by: C_1 ($r = 0.64$), N_{704} ($r = 0.61$) and RE_1 ($r = 0.59$) (table 6). Moderate correlations were found between chlorophyll levels and these indices: R_o (Chl a $r = -0.61$, Chl b $r = -0.65$ and Chl $(a+b)$ $r = -0.62$), N_{693} (Chl a $r = -0.61$, Chl b $r = -0.63$ and Chl $(a+b)$ $r = -0.62$) and N_{704} (Chl a $r = -0.61$, Chl b $r = -0.64$ and Chl $(a+b)$ $r = -0.62$). $RARS_c$ was related to carotenoid levels ($r = 0.75$) and to the ratio Chl $(a+b)/N$ ($r = 0.71$) (table 6).

The correlations of the IGM parameters (R_s and R_o) and the $RARS_c$ index to pigments (table 6) have been reported previously (Miller *et al.* 1990, Datt 1998). Our findings demonstrate that a strong relationship exists between several of the reflectance indices and foliar lignin and non-polar compounds, not documented by previous studies. This strong correlation provides the physiologically based link for use of the reflectance indices R_o , C_1 , RE_1 , N_{704} , D_{\max}/D_{704} and $RARS_c$ for the evaluation of forest damage condition.

4. Conclusions

This study demonstrates that hyperspectral data can provide improved forest damage separation capabilities when compared to multispectral broadband data. In the visible and red-edge region a general trend in the Norway spruce canopy spectra of increasing canopy reflectance intensity with increasing damage levels was detected by ASAS, while in the near infrared the opposite spectral trend was evident—the healthy (DC0) stands had the highest reflectance. Such a spectral pattern appears typical at foliar and canopy scales for Norway spruce in decline. Using ASAS 10 nm airborne canopy reflectance, the 673–724 nm spectrum provided the highest potential for identifying the forests with initial levels of damage

Table 6. Correlation between ASAS spectral indices with highest potential for damage separation and the canopy pigments and chemical constituents ($n=23$, correlation coefficients).

Indices	Correlation to pigments				Correlation to foliar chemistry			
	Chl a	Chl b	Chl $(a+b)$	Chl $(a+b)/N$	Lignin	Cellulose	Polar	Non-polar
C_1 (R_{693}/R_{775})	-0.52	-0.55	-0.53	-0.50	-0.69¹	-0.60	0.64	0.84
RE_1 ($Av(R_{673}...R_{703.8})$)	-0.47	-0.52	-0.48	-0.46	-0.66	-0.55	0.59	0.88
$RARS_c$ (R_{775}/R_{502})	0.56	0.57	0.56	0.71	0.24	-0.10	0.02	-0.45
N_{693}	-0.61	-0.63	-0.62	-0.52	-0.54	-0.50	0.54	0.61
N_{704}	-0.61	-0.64	-0.62	-0.53	-0.61	-0.57	0.61	0.71
D_{714}/D_{704}	0.25	0.24	0.25	0.17	0.53	0.32	-0.43	-0.49
D_{\max}/D_{704}	0.16	0.17	0.16	0.09	0.47	0.25	-0.29	-0.69
R_s	-0.43	-0.49	-0.44	-0.39	-0.45	-0.25	0.30	0.73
R_o	-0.61	-0.65	-0.62	-0.56	-0.67	-0.47	0.54	0.87

¹The highest correlations between spectral index and canopy biophysical parameter are in bold.

(separation of DC0 and DC1). Nine spectral indices were identified as strongly correlated to damage. These high spectral resolution indices (three band ratios, two normalized red edge bands, two derivative indices, and two modelled parameters of inverted Gaussian model) present the most potential for use as spectral indicators of the initial level of damage. Derivative indices were identified as least sensitive to vegetation morphological parameters, therefore providing high potential for across-forest scales and across-instruments comparisons. However, the derivative indices computed from the 10 nm ASAS bands were found to be marginal for discriminating forest damage classes and it is anticipated that a higher spectral resolution would increase the success.

The most reliable field indicator of forest damage was the number of needle age-classes retained (declining with increasing damage level), which demonstrates the importance for RS monitoring of forest health to apply spectral methods evaluating the changes in foliar amount and biophysical properties. Across the damage gradient, from DC0 to DC3, foliar pigment levels were relatively stable, while the forest damage gradient had a significant effect on the foliar chemical constituents. This finding suggests the possibility of a forest health condition in which foliar pigments at the heavily damaged forests (DC3) have recovered to levels close to the concentrations occurring in healthy forest (DC0) stands, while foliar chemical constituents may reflect the long-term health condition of these forests. This study documents the potential of the chlorophyll *a/b* ratio as a bio-indicator of short-term damage, and establishes the high potential of foliar chemical compounds as indicators of long-term forest health.

The strong relationships between the reflectance indices and foliar chemistry (pigments as well as lignin, polar and non-polar compounds) provide the biophysiological link for use of the indices as spectral indicators of forest damage.

Acknowledgments

We wish to acknowledge the support the NASA Terrestrial Ecology Program, which funded this research.

We thank J. Rajl (Nature Conservancy and Landscape Protection Agency, Czech Republic) and the team of students from Charles University, Prague, Czech Republic for assisting in our field efforts. We are grateful to V. Henzlik (Forest Management Institute, Czech Republic) for his guidance in the Krusne hory forests.

References

- ACCP, 1994, Accelerated Canopy Chemistry Program: Final Report Presented to EOS-IWG, 19 October 1994, USA.
- ARDO, J., LAMBERT, N., HENZLIK, V., and ROCK, B. N., 1997, Satellite-based estimations of coniferous forest cover changes: Krusne hory, Czech Republic 1972–1989. *Ambio*, **26**, 158–166.
- BLACKBURN, G. A., 1998, Spectral indices for estimating photosynthetic pigment concentrations: a test using senescent tree leaves. *International Journal of Remote Sensing*, **19**, 657–675.
- BOLSTER, K. L., MARTIN, M. E., and ABER, J. D., 1996, Determination of carbon fraction and nitrogen concentration in tree foliage by near infrared reflectance: a comparison of statistical methods. *Canadian Journal of Forest Research*, **26**, 590–600.
- BOOCHS, F., KUPFER, G., DOCKTER, K., and KÜHBAUCH, W., 1990, Shape of the red edge as vitality indicator for plants. *International Journal of Remote Sensing*, **11**, 1741–1753.
- CARTER, G. A., 1994, Ratios of leaf reflectance in narrow wavebands as indicators of plant stress. *International Journal of Remote Sensing*, **15**, 697–703.
- CARTER, G. A., REBBECK, J., and PEARCY, K., 1995, Leaf optical properties in *Liriodendron*

- tulipifera* and *Pinus strobus* as influenced by increased atmospheric ozone and carbon dioxide. *Canadian Journal of Forest Research*, **25**, 407–412.
- CARTER, G. A., DELL, T. R., and CIBULA, W. G., 1996, Spectral reflectance characteristics and digital imagery of a pine needle blight in the southern U.S. *Canadian Journal of Forest Research*, **26**, 402–407.
- CHAPPELLE, E. W., KIM, M. S., and MCMURTREY, J. E., 1992, Ratio analysis of reflectance spectra (RARS): an algorithm for the remote estimation of the concentrations of chlorophyll a, chlorophyll b, and carotenoids in soybean leaves. *Remote Sensing of Environment*, **39**, 239–247.
- DABNEY, P. W., TIERNEY, M. R., IRONS, J. R., KOVALICK, W. M., BUR, M. J., and RUSSELL, C. A., 1999, Inter-comparison of sensor calibration techniques for the Advanced Solid-state Array Spectroradiometer (ASAS) as a performance validation tool. *SPIE Proceedings*, **3750**, 442–452. SPIE 18–20 July 1999, Denver, Earth Observing systems IV.
- DATT, B., 1998, Remote sensing of chlorophyll a, chlorophyll b, chlorophyll a + b, and total carotenoid content in eucalyptus leaves. *Remote Sensing of Environment*, **66**, 111–121.
- DEERING, D. W., MIDDLETON, E. M., and ECK, T. F., 1994, Reflectance anisotropy for a spruce-hemlock forest canopy. *Remote Sensing of Environment*, **47**, 242–260.
- DEERING, D. W., ECK, T. F., and BANERJEE, B., 1999, Characterization of the reflectance anisotropy of three boreal forest canopies in spring–summer. *Remote Sensing of Environment*, **67**, 205–229.
- DICKINSON, R. E., 1984, Modeling evapotranspiration for three-dimensional global climate models. *Climate Processes and Climate Sensitivity, Geophysical Monographs*, **29**, American Geophysical Union, 58–72.
- EKSTRAND, S., 1996, Landsat TM-based forest damage assessment: correction for topographic effects. *Photogrammetric Engineering and Remote Sensing*, **62**, 151–161.
- ELVIDGE, C. D., and CHEN, Z., 1995, Comparison of broad-band and narrow-band red and near-infrared vegetation indices. *Remote Sensing of Environment*, **54**, 38–48.
- ENTCHEVA, P. K., 2000, Remote sensing of forest damage in the Czech Republic using hyperspectral methods. (Ph.D. Thesis, University of New Hampshire, Durham, USA).
- ENTCHEVA, P. K., ROCK, B. N., LAUTEN, G., and CIBULA, W., 1996, Remote sensing assessment of forest health in the Bohemian forests of central Europe. *Global Networks for Environmental Information, ECO-INFORMA '96*, **11**, 785–790.
- FIELLA, I., AMARO, T., ARAUS, J. L., and PEÑUELAS, J., 1996, Relationship between photosynthetic radiation-use efficiency of barley canopies and the photochemical reflectance index (PRI). *Physiologia Plantarum*, **96**, 211–216.
- GAMON, J. A., PEÑUELAS, J., and FIELD, C. B., 1992, A narrow-waveband spectral index that tracks diurnal changes in photosynthetic efficiency. *Remote Sensing of Environment*, **41**, 35–44.
- GAMON, J. A., SERRANO, L., and SURFUS, J. S., 1997, The photochemical reflectance index: an optical indicator of photosynthetic radiation use efficiency across species, functional types and nutrient levels. *Oecologia*, **112**, 492–501.
- HENZLIK, V., 1997, Personal communication of B. N. Rock and P. K. Entcheva.
- HILDEBRANDT, G., and GROSS, C., 1992, Manual for remote sensing forest health status assessment. (Development funded by European Union, Commission for Agriculture, Grant 89.06.CO.03. Belgium: Walpot SA).
- HORLER, D. N. H., DOCKRAY, M., BARBER, J., and BARRINGER, A. R., 1983, Red edge measurements for remotely sensing plant chlorophyll content. *Advances in Space Research*, **3**, 273–277.
- IRONS, J. R., RANSON, K. J., WILLIAMS, D. L., IRISH, R. R., and HUEGEL, F. G., 1991, An off-nadir-pointing imaging spectroradiometer for terrestrial ecosystem studies. *IEEE Transactions on Geoscience and Remote Sensing*, **29**, 66–74.
- JORDAN, R. J., 1969, Derivation of leaf area index from quality of light on the forest floor. *Ecology*, **50**, 663–666.
- KIMES, D. S., NEWCOMB, W. W., NELSON, R. F., and SCHUTT, J. B., 1986, Directional reflectance distributions of a hardwood and pine forest canopy. *IEEE Transactions on Geoscience and Remote Sensing*, **GE-24**, 281–293.
- KLASTERSKA, I., 1991, Bohemian problem bared. *Acid News*, **1**, 1–4.
- KLIMONT, Z., AMANN, M., COFALA, J., GYARFAS, K., LAASSEN, G., and SCOPP, W., 1993,

- Emission of air pollutants in the region of Central Europe Initiative* (Laxenburg, Austria: IIASA).
- KOVALICK, W. M., GRAHAM, D. W., and BUR, M. J., 1994, Data processing and calibration of the Advanced Solid-state Array Spectrometer. In *Proceedings of the IEEE Transactions on Geoscience and Remote Sensing Symposium*, **3**, 1652–1654.
- KRIEBEL, K. T., 1978, Measured spectral bidirectional reflectance properties of four vegetated surfaces. *Applied Optics*, **17**, 253–259.
- KUBIKOVA, J., 1991, Forest dieback in Czechoslovakia. *Vegetatio*, **93**, 101–108.
- LAMBERT, N. J., ARDO, J., ROCK, B. N., and VOGELMANN, J. E., 1995, Spectral characterization and regression based classification of forest damage in Norway spruce stands in the Czech Republic using Landsat Thematic Mapper data. *International Journal of Remote Sensing*, **16**, 1261–1287.
- LICHTENTHALER, H. K., 1988, *Applications of chlorophyll fluorescence in photosynthesis research, stress physiology, hydrology and remote sensing* (Dordrecht, The Netherlands: Kluwer Academic).
- MARTIN, M. E., 1994, Measurements of foliar chemistry using laboratory and airborne high spectral resolution visible and infrared data (Ph.D. Thesis, University of New Hampshire, Durham).
- MARTIN, M. E., and ABER, J. D., 1997, High spectral resolution remote sensing of forest canopy lignin, nitrogen, and ecosystem processes. *Ecological Applications*, **7**, 431–443.
- MATERNA, J., 1989, Air pollution and forestry in Czechoslovakia. *Environmental Monitoring and Assessment*, **12**, 227–235.
- M McNULTY, S. G., ABER, J. D., McLELLAN, T. M., and KATT, S. M., 1991, Nitrogen cycling in high elevation forests in the northeastern U.S. in relation to nitrogen deposition. *Ambio*, **19**, 38–40.
- MIDDLETON, E. M., 1992, Quantifying reflectance anisotropy for photosynthetically active radiation in grasslands. *Journal of Geophysical Research*, **97**, 18935–18946.
- MILLER, J. R., HARE, E. W., and WU, J., 1990, Quantitative characterisation of the vegetation red edge reflectance. 1: An Inverted-Gaussian reflectance model. *International Journal of Remote Sensing*, **11**, 1755–1774.
- MILLER, J. R., FREEMANTLE, J. R., BELANGER, M. J., ELVIDGE, C. D., and BOYER, M. G., 1990, Potential for determination of leaf chlorophyll content using AVIRIS. *1990 Proceedings of the Second Airborne Visible/Infrared Imaging Spectrometer (AVIRIS) Workshop*. 72–77, Pasadena, CA, 4–8 June 1990.
- MOSS, D. M., and ROCK, B. N., 1991, Analysis of red edge spectral characteristics and total chlorophyll values for red spruce (*Picea rubens*) branch segments from NH. Moosilauke, NH, USA. *IGARSS '91 Proceedings*, **3**, 1529–1532.
- MOSS, D. M., ROCK, B. N., BOGLE, A. L., and BILKOVA, J., 1998, Anatomical evidence of the development of damage symptoms across a growing season in needles of red spruce from central New Hampshire. *Environmental and Experimental Botany*, **39**, 247–262.
- NAPAP, 1990, State of science and technology. (National Acidic Precipitation Assessment Program, Integrated Report, **3**, 556, USA).
- NEWMAN, S. D., SOULIA, M. E., ABER, J. D., DEWEY, B., and RICCA, A., 1994, Analyses of forest foliage: Laboratory procedures for proximate carbon fractionation and nitrogen determination. *Journal of Near Infrared Spectroscopy*, **2**, 5–14.
- PEÑUELAS, J., and FIELLA, I., 1998, Visible and near-infrared reflectance techniques for diagnosing plant physiological status. *Trends in Plant Science*, **3**, 151–156.
- PORRA, R. J., THOMPSON, W. A., and KRIEDEMANN, P. E., 1989, Determination of accurate extinction coefficients and simultaneous equations for assaying chlorophylls *a* and *b* extracted with four different solvents: verification of the concentration of chlorophyll standards by atomic absorption spectroscopy. *Biochimica et Biophysica Acta*, **975**, 384–394.
- RANSON, K. J., IRONS, J. R., and DAUGHTRY, C. S., 1991, Surface albedo from bidirectional reflectance. *Remote Sensing of Environment*, **35**, 201–211.
- ROCK, B. N., VOGELMANN, J. E., WILLIAMS, D. L., VOGELMANN, A. F., and HOSHIZAKI, T., 1986, Remote detection of forest damage. *BioScience*, **36**, 439–445.
- ROCK, B. N., HOSHIZAKI, T., and MILLER, J. R., 1988, Comparison of *in situ* and airborne spectral measurements of the blue shift associated with forest decline. *Remote Sensing of Environment*, **24**, 109–127.

- ROCK, B. N., GRECZYNSKI, J., MOSS, D. M., and ZAWILA-NIEDZWICKI, T., 1992, Spectral characterization of forest decline damage in branch segments of Norway spruce (*Picea abies*) in the Sudety Mountains of Poland. *Proceedings of the American Society of Photogrammetry and Remote Sensing*, **1**, 271–279.
- ROCK, B. N., SKOLE, D. L., and CHOUDHURY, B. J., 1993, Monitoring vegetation change using satellite data. In *Vegetation Dynamics and Global Change*, edited by A. M. Solomon and H. H. Shugart (New York: Chapman & Hall), pp. 153–167.
- RUSSELL, C. A., IRONS, J. R., and DABNEY, P., 1997, Bidirectional reflectance of selected BOREAS sites using the new ASAS Sensor array. *Journal of Geophysical Research*, **102** (D24): **29**, 505–529, 516.
- TANRE, D., DEUZE, J. L., HERMAN, M., VERMOTE, E. F., and HORCRETTE, J. J., 1997, Second simulation of the satellite signal in the solar spectrum 6S: an overview. *IEEE Transactions of Geoscience and Remote Sensing*, **35**, 675–686.
- VOGELMANN, J. E., ROCK, B. N., and MOSS, D. M., 1993, Red edge spectral measurements in sugar maple leaves. *International Journal of Remote Sensing*, **14**, 1563–1575.
- WARING, R. H., and RUNNING, S. W., 1998, *Forest Ecosystems: Analysis at Multiple Scales* (San Diego, CA: Academic Press, Harcourt Brace & Company).
- WELLBURN, A. R., 1994, The spectral determination of chlorophylls *a* and *b*, as well as total carotenoids, using various solvents with spectrophotometers of different resolution. *Journal of Plant Physiology*, **144**, 307–313.
- WILLIAMS, P., and NORRIS, K., 1987, *Near-infrared technology in the agricultural and food industries* (St. Paul, MN: American Association of Cereal Chemists).
- ZAR, J., 1996, *Biostatistical Analysis* (Upper Saddle River, NJ: Prentice Hall).
- ZARCO-TEJADA, P. J., MILLER, J. R., MOHAMMED, G. H., NOLAND, T. L., and SAMPSON, P. H., 1999, Optical indices as bio-indicators of forest condition from hyperspectral CASI data. *Remote Sensing in the 21st Century: Economic and Environmental Applications, Proceedings of the 19th (EARSel) Symposium on Remote Sensing in the 21st Century*, Valladolid, Spain, 31 May–2 June 1999, edited by J. L. Casanova (Rotterdam: Balkema), pp. 517–522.